PHYSICS

Anomalous excitations of atomically crafted quantum magnets

Sascha Brinker[1]*, Felix Küster[2], Stuart S. P. Parkin[2], Paolo Sessi[2], Samir Lounis[1,3]*

High–energy resolution spectroscopic studies of quantum magnets proved extremely valuable in accessing magnetodynamics quantities, such as energy barriers, magnetic interactions, and lifetime of excited states. Here, we investigate a previously unexplored flavor of low-energy spin excitations for quantum spins coupled to an electron bath. In sharp contrast to the usual tunneling signature of two steps symmetrically centered around the Fermi level, we find a single step in the conductance. Combining time-dependent and many-body perturbation theories, magnetic field–dependent tunneling spectra are explained as the result of an interplay between weak magnetic anisotropy energy, magnetic interactions, and Stoner-like electron-hole excitations that are strongly dependent on the magnetic states of the nanostructures. The results are rationalized in terms of a noncollinear magnetic ground state and the dominance of ferro- and antiferromagnetic interactions. The atomically crafted nanomagnets offer an appealing model for the exploration of electrically pumped spin systems.

INTRODUCTION

Atomic-scale magnetodynamics is at the cornerstone of spin-based nanoscale devices for future information technology. It defines how and on which time scales magnetic states can be controllably manipulated. The interaction of local spins with the local environment plays a crucial role in determining their properties. Orbital hybridization effects, charge transfer, and the presence of nearby impurities have all been reported to strongly affect the magnetic ground state, ultimately determining a range of magnetodynamic quantities, including magnetic anisotropy, spin lifetime, and spin relaxation mechanisms (*1*–*13*). The development of experimental techniques capable of directly capturing these properties in reduced dimensions allows one to visualize the breakdown of classical or semiclassical descriptions of magnetic phenomena at subnanometer scales, revealing the emergence of exquisite quantum mechanical effects (*14*–*19*). These achievements enabled the understanding of the ultimate limits of classical computational schemes while simultaneously setting the ground for testing ideas and concepts that might find direct application in innovative spin-based quantum computational schemes (*2*, *20*–*23*).

In this context, scanning tunneling spectroscopy (STS) techniques occupy a primary role. They were particularly instrumental in detecting not only several ground-state phenomena but also a wealth of fundamental excitations such as those with magnetic (*6*, *7*, *9*, *15*, *24*–*29*), vibrational (*30*), polaronic (*31*), excitonic (*32*), or Kondo characteristics (*14*, *24*, *33*–*36*). The analysis of the distinct spectral shapes identified in tunneling transport sheds light on their origin and ideally a link to a specific excitation process. For instance, measurements in an applied magnetic field have proven extremely useful in disentangling magnetic and nonmagnetic excitations. However, dissimilar and, in some cases, competing processes can be simultaneously at play, which can make the analysis complicated. This requires a careful theoretical-experimental investigation to unveil the fundamental mechanisms at play.

The Kondo effect versus spin-excitation paradigm is a particularly intriguing case (*37*–*40*). Both phenomena share a similar magnetic origin. However, they are profoundly different in nature, ultimately leading to opposing technological implications. On the one hand, spin excitations emerge from the promotion of a magnetic moment from its ground state to various excited states. Since spin excitations play a crucial role in how magnetic bits are written, understanding these processes is key in information technology. In tunneling experiments, inelastic spin excitations are expected to appear in the differential conductance as symmetric steps centered around the Fermi energy, which shift in energy in response to an applied magnetic field (*24*). Their spectral shape encodes information directly related to the reading and manipulation of spins, such as the lifetime of the excited states and the related energy barriers (e.g., the magnetic anisotropy energy) (*4*, *6*, *7*, *15*). On the other hand, the Kondo effect emerges from the entanglement of the spin of an atom with that of the surrounding bath of electrons (*33*, *34*), which leads to many-body screening of the spin below the energy scale defined by the Kondo temperature. Consequently, although of great fundamental interest in the context of many-body physics, the Kondo effect is of limited technological importance. Spectroscopically, the Kondo effect is revealed in complicated spectral shapes that are generally analyzed as Fano resonances (*14*, *35*, *36*). Consequently, a clear identification of the underlying mechanisms is often complex since many fitting parameters need to be used, especially when multiorbitals are involved (*41*, *42*). There are several examples, where the same spectral shape is found whether one invokes a Kondo effect or simply considers the molecular/atomic orbitals or a combination of both, which sometimes can be arbitrary (*40*, *43*–*45*). In this context, recent ab initio simulations challenged the Kondo versus conventional spin-excitation picture. By including spin-orbit coupling, the well-known zero-bias anomalies experimentally observed for Co adatoms on Cu, Ag, and Au surfaces (*40*) were systematically explained as gapped unconventional spin excitations, calling for new experiments to verify their origin.

In this contribution, we report on the emergence of anomalous spectroscopic signatures centered around the Fermi energy for Cr single atoms coupled to metallic niobium, their magnetic field dependence, and their evolution once adatoms are coupled through

[1]Peter Grünberg Institut and Institute for Advanced Simulation, Forschungszentrum Jülich and JARA, Jülich D-52425, Germany. [2]Max Planck Institute of Microstructure Physics, Halle 06120, Germany. [3]Faculty of Physics, University of Duisburg-Essen and CENIDE, 47053 Duisburg, Germany.
*Corresponding author. Email: s.brinker@fz-juelich.de (S.B.); s.lounis@fz-juelich.de (S.L.)

the creation of atomically crafted antiferromagnetic and ferromagnetic nanostructures. Although their spectral shape might be reminiscent of Kondo resonances, our first-principles simulations identify them as new paradigmatic spectroscopic manifestations of spin excitations. While the observation of spin excitations of antiferromagnetic multispin nanostructures has so far been explored to a great extent on thin insulating substrates [see e.g., (*15*, *17*, *18*)] and has been elusive on metals, here we demonstrate on a metallic substrate the design of antiferromagnetic or ferromagnetic magnets composed of a few exchange-coupled Cr atoms that enables the tailoring of the shape and linewidth of the corresponding spectroscopic features, which are intimately linked to the adatoms' weak magnetic anisotropy energy and the strong dependence of the excitation lifetime on the underlying magnetic texture.

RESULTS

Adatoms

As a prototypical platform, we focus on Cr atoms coupled to the (110) surface of Nb. The Nb crystal was prepared according to the procedures described in (*46*). Single Cr adatoms were deposited directly onto a cold substrate, as described in Methods. All atoms are found to be adsorbed in hollow stacking sites, which are energetically most favorable (*47*). Figure 1A shows a region of the Nb surface where blue dots correspond to Cr adatoms. After deposition, atomic manipulation has been used to create a nanostructure with an isolated Cr atom, which is well separated (distance, > 6 nm) from all surrounding atoms as shown in Fig. 1A. This allows us to analyze the effect of local magnetic moments coupled to an electron bath, while excluding the influence of nearby adatoms, which can couple to each other by indirect interactions mediated by the conduction electrons, i.e., the RKKY coupling, ultimately influencing the magnetic adatom ground state (*48*).

Figure 1B shows a sequence of spectra, measured in a small energy range centered around the Fermi level, where the tip was positioned directly on top of the Cr adatom. All spectroscopic data have been acquired in the presence of a magnetic field applied perpendicular to the sample surface. Starting from a value of 1 T, which is necessary to drive the otherwise superconducting Nb substrate (T_c = 9.3 and B_c = 0.8 T) into the normal metallic regime, the strength of the magnetic field is progressively increased up to 6. This procedure allows us to map the evolution of the spectroscopic data and to assess the magnetic origin of the excitations. The dI/dU spectra are characterized by an asymmetric step-like feature around the Fermi level, which shows a substantial magnetic field dependence. The step starts at negative bias voltage and reaches its maximum at positive bias. By increasing the magnetic field, the step broadens. Moreover, an additional feature emerges at negative voltage starting from 3 T. This effect is more seen by looking at the derivative (d^2I/dU^2) reported in Fig. 1C, where the magnetic field–dependent broadening is visible. At the maximum magnetic field available in our setup, the broadening appears to split into two distinct features symmetrically centered around the Fermi level (additional experimental plots and fits are presented in notes S2 to S4). As described in the following, spin excitations can account for both the spectral shape as well as its magnetic field dependence.

To explore the origin of the anomalous spectral feature, we use a combination of relativistic time-dependent density functional theory (TD-DFT) and many-body perturbation theory (MBPT) implemented in the framework of the Korringa-Kohn-Rostoker Green function

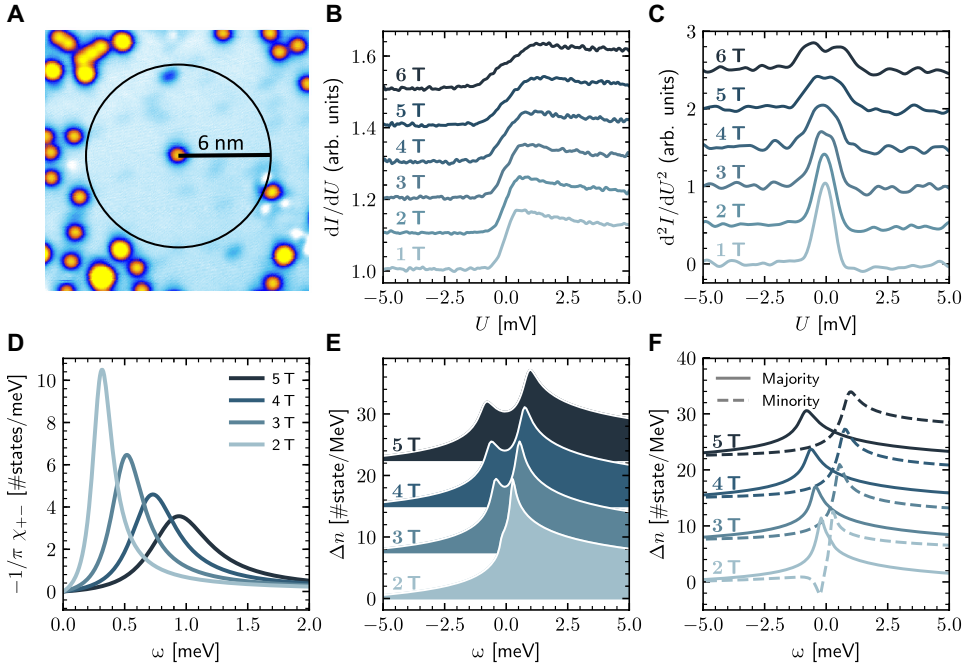

Fig. 1. Experimental and theoretical inelastic STS fingerprint of a Cr adatom on the Nb(110) surface with varying external magnetic fields. (**A**) Experimental topography image of the adatom. (**B** and **C**) Experimental dI/dU and d^2I/dU^2 spectra, I = 3 nA, and T = 600 mK. (**D**) Density of spin-flip excitations obtained from TD-DFT. (**E**) Theoretical inelastic STS spectrum corresponding to the renormalized local density of states from MBPT calculated at a height of 4.7 Å above the adatom. (**F**) Similar to (E) with the spin-resolved theoretical spectra. The different field-dependent spectra are shifted to improve visibility.

method (*40*, *49*) (see Methods). The ab initio nature of the theoretical approach allows us to address the investigated spectroscopic phenomena without the use of adjusting parameters. Thus, we do not perform or rely on a fitting procedure of the experimental data. This framework is ideal to treat the ground state and spin-excited state of adatoms on surfaces as shown in various studies (*6*, *7*, *27*) and their theoretical inelastic tunneling spectra (*40*, *49*, *50*). The Cr adatom carries a spin moment of 3.53 μ_B characterized by a weak magnetic anisotropy energy, 0.20 mcV, slightly favoring an in-plane orientation of the magnetic moment (the local density of states is presented in note S1). However, in the presence of a magnetic field perpendicular to the substrate, the spin moment points out-of-plane. Owing to the weak magnetic anisotropy of the Cr spin moment, it can be excited by the tunneling electrons at very low energies. Our theory allows us to effectively capture these processes by quantifying the excitation probability in terms of the density of spin-flip excitations, which can be extracted from the imaginary part of the transverse spin-spin susceptibility, $-1/\pi\ \mathrm{Im}\,\chi_{+-}(\omega)$, shown in Fig. 1D. The density of spin excitations encodes two main features: (i) the energy of the spin excitation ω_0 directly related to the magnetic anisotropy energy and applied magnetic field and (ii) their lifetime, which is inversely proportional to the broadening (full width half maximum). The origin of this broadening is Stoner-like electron-hole excitations provided by the highly itinerant electrons of the metallic substrate. Such single-particle excitations are emitted while strongly contributing to the decay of spin excitations (*6*, *51*).

In contrast to a scenario where the adatoms are deposited on an insulator, the magnetic moments on a metal experience additional effects with respect to usual interactions forming a Heisenberg Hamiltonian such as the magnetic anisotropy, Zeeman energy, and magnetic exchange interactions. The reason is the nature of electron-forming moments, which are delocalized and extend beyond the atomic site, and thus do not respond uniformly to external perturbation. Therefore, while the magnetic moment undergoes a spin-flip process, which is by nature a collective excitation process involving many electrons, single-particle excitations, wherein a single electron may be excited from a majority-spin state below the Fermi level to a minority-spin state above, kick in and affect the overall dynamical behavior of the magnetic moment. The inhomogeneous reaction of the electrons broaden then the ideal response of the spin moment, leading to an effective decay, or damping, of the spin excitation. We note that such electron-hole excitations are associated with spin currents discussed in the context of spin-pumping experiments (*52*–*54*). The larger the number of electron-hole excitations, the stronger the damping and the shorter is the lifetime of the spin-excited states. As can be recognized from Fig. 1D, our model effectively accounts for all experimental trends, both in the energy shift and in the broadening (Fig. 1, B and C).

When the magnetic moment of the atom is excited, the triggered spin excitations affect the electron density, resulting in the spectroscopic signatures visible in the theoretically calculated tunneling spectra reported in Fig. 1E, which are obtained from a many-body perturbation theory (see Methods). In good agreement with the experimental measurements, we recover a step-like signature of the spin excitation with a clear field-dependent broadening, which progressively evolves toward a double peak structure at high magnetic field. The origin of this behavior is effectively captured in Fig. 1F, which illustrates the magnetic field evolution of the spin-resolved tunneling spectra for majority (continuous line) and minority (dashed line) spins. A single peak feature at negative energies and a step-like function with onset at positive energies are visible for majority and minority spin channels, respectively. The energy separation between the majority and minority spectral signatures becomes larger by progressively increasing the strength of the magnetic field. We note that besides Cr adatom, Mn also displays a similar but weaker step-like zero-bias anomaly, which is nicely reproduced by our ab initio simulations as shown in note S5.

To analytically grasp the connection between the various magneto-dynamical parameters shaping the unveiled spectroscopic anomalies, it is useful to map the TD-DFT results to the equation of motion of a spin moment, the Landau-Lifshitz-Gilbert equation (*55*–*57*), $\frac{\mathrm{d}\mathbf{M}}{\mathrm{d}t} = \gamma\mathbf{M} \times \frac{\mathrm{d}H}{\mathrm{d}\boldsymbol{M}} + \frac{\alpha}{M}\mathbf{M} \times \frac{\mathrm{d}\mathbf{M}}{\mathrm{d}t}$, subjected to a Heisenberg Hamiltonian H (more details are given in Methods and notes S6 and S8). The field dependence of the excitation energy obeys $\omega_0 = \gamma'(\mathcal{K} + BM)/M$, while the broadening (inverse lifetime) of the excitation is given by $\alpha\gamma'(\mathcal{K} + BM)/M$, where $\mathcal{K}$ is the magnetic anisotropy energy, which represents the costs in energy in rotating the magnetic moments from z toward the x and y directions (corresponding to the $[1\bar{1}0]$ and [001] directions, respectively). M is the magnetic moment, B is an out-of-plane magnetic field, γ' is the renormalized gyromagnetic ratio, and α is the so-called Gilbert damping parameter, which quantifies the probability of creating electron-hole excitations responsible for the decay of the spin excitations. This theoretical description allows us to effectively capture the following trends: (i) The excitation energy becomes higher by increasing the strength of the magnetic field acting on the magnetic moment, and (ii) this is accompanied by the damping that becomes progressively stronger by enhancing the amplitude of the electron-hole excitations. Overall, this approach allows the visualization of the existence of competing trends in the manifestation of spin excitations. While an enhanced magnetic anisotropy facilitates their detection, it also simultaneously enables the creation of more electron-hole pairs, increasing the broadening, ultimately washing out their spectroscopic signature. Overall, this could explain why identifying the spin-excitation origin of similar spectra observed for Co on Cu(001) and Ag(001) surfaces (*35*, *40*, *58*), characterized by a larger magnetic anisotropy energy than for Cr on Nb(110), is challenging since this requires extremely large magnetic fields and therefore has escaped experimental observation to date.

Dimers

To further explore the consistency of the experimental data with the spin-excitation paradigm, we use atomic manipulation techniques to artificially create magnetic dimers oriented along different crystallographic directions on the Nb(110) surface. We consider three next-nearest neighbor configurations: $[1\bar{1}0]$, $[1\bar{1}1]$, and [001], illustrated in Fig. 2A. The highly anisotropic (110) surface enables us to create and scrutinize distinct direction-dependent magnetic ground states using the coupling between the adatoms mediated by the conduction electrons. This effect is expected to be directly imprinted in the spin-excitation spectra, which should show a clear direction dependence. STS measurements confirm the existence of a strong direction-dependence behavior, as visible in Fig. 2B. A single step-like spectroscopic signature centered around the Fermi level is visible for all the three distinct directions. However, a strong direction-dependent deviation with respect to the signal obtained for the isolated single Cr atom is evident, both in the intensity and in the

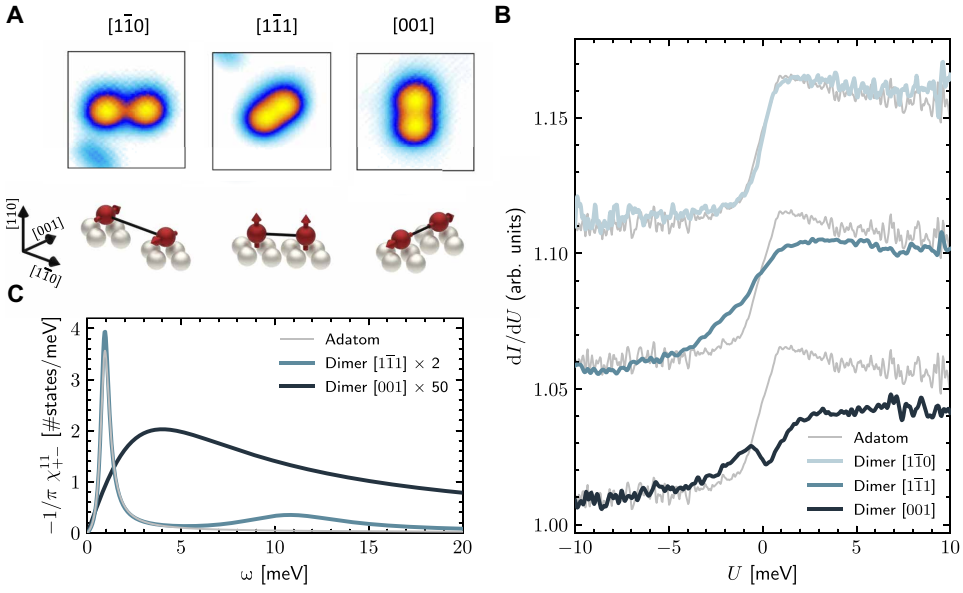

Fig. 2. Theoretical and experimental inelastic STS fingerprint of the Cr dimers along the [001], [1$\bar{1}$0], and [1$\bar{1}$1] directions on the Nb(110) surface. (**A**) Illustration of the dimers (STM topography) and its ground-state magnetic structures. The magnetic structures are obtained from self-consistent noncollinear DFT calculations. (**B**) Experimental inelastic STS spectra of the dimers, I = 3 nA and T = 600 mK (colored lines). The measurements on the single Cr adatom are shown as reference (thin gray lines; see also Fig. 1). The different spectra are vertically shifted to improve visibility. (**C**) Magnetic susceptibility obtained from TD-DFT. The spectra of the [001] and [1$\bar{1}$1] dimer are scaled by a factor of 50 and 2, respectively.

broadening. The [1$\bar{1}$0] dimer is characterized by the largest separation and therefore the weakest coupling between the adatoms, resulting in only very minor differences with respect to the isolated atom case. In sharp contrast, both the [1$\bar{1}$1] and the [001] dimers show a substantial broadening of the step-like feature. The spectrum corresponding to the [001] dimer hosts a deep-like feature offset from zero bias, surrounded by two maxima that are not symmetrically located with respect to the Fermi energy. In general, these observations are in line with the theoretically calculated strength of the magnetic exchange interactions along different crystallographic directions summarized in Table 1.

In the following, we present a theoretical analysis, which allows us to effectively understand the origin of the distinct behavior observed for dimers aligned along the [1$\bar{1}$1] and [001] directions, where the magnetic coupling is the strongest. Since the adatoms are not nearest neighbors, the single ion anisotropy of each of the adatoms remains constant (see Table 1). However, the nature of the coupling is opposite along the two different directions, resulting in a strong antiferromagnetic (7.94 meV) and ferromagnetic interaction (−8.95 meV) for [001] along the [1$\bar{1}$1] direction, respectively. These predictions are in line with the experimental observations reported in note S11, where the magnetic coupling between next-nearest neighbor adatoms has been scrutinized by using a functionalized superconducting tip [a similar approach was introduced in (*59*)]. As demonstrated in the "Adatoms" subsection, the analysis of the spin-excitation spectra can be carried out on the basis of the density of spin-flip excitations, which provide the intrinsic inelastic spectra. These are obtained from the first-principles ground states illustrated in Fig. 2A, resulting from the interplay of the single ion anisotropy, magnetic exchange interaction, and magnetic field. The density of spin excitations is shown and compared to that of the isolated Cr adatom in Fig. 2C for each of the atoms forming the dimers.

Since the [1$\bar{1}$1] dimer is ferromagnetic (see Fig. 2A and note S7), the density of spin excitation hosts a double peak structure, leading to a redistribution of the spectral weight observed for the isolated adatom. They represent the acoustical and optical excitation modes, where, in a classical picture, the spin moments precess either clockwise or counterclockwise, respectively. A simple description based on a quantum spin model is given in note S9. The position of the lowest mode, also observed experimentally, is dictated by the magnitude of the magnetic anisotropy energy ($\gamma'\mathcal{K}/M$) and shows a weaker intensity than that of the excitation mode of the isolated adatom with a broadening given by $\gamma'\alpha\mathcal{K}/M$ (see note S8). The optical mode, however, occurs at energies not resolvable within the experiment since it is dictated by the magnitude of the exchange interaction $\gamma'(\mathcal{K}-J)/M$, leading to a much broader feature ($\gamma'\alpha(\mathcal{K}-J)/M$) than the acoustical one.

In contrast to the ferromagnetic dimer, the antiferromagnetic one exhibits a single broad mode settled by the magnetic exchange interaction $\left(\gamma'\sqrt{4\mathcal{K}(\mathcal{K}+J)-\alpha^2(J-2\mathcal{K})^2}/2M\right)$ since the excitation process promotes the dimer from a state where the total spin is 0 to 1. The broadening of the state is given by $\gamma'\alpha(2\mathcal{K}+J)/2M$, which explains the large damping observed in both the experimental and theoretical spectra shown for the [001] dimers in Fig. 2 (B and C).

Overall, our theoretical analysis highlights that antiferromagnetic dimers are subjected to stronger electron-hole excitations, resulting in spin excitations characterized by larger energy broadening, i.e., shorter lifetimes, compared to the ferromagnetic case. This behavior manifests itself in a larger energy broadening along the [001] direction as compared to the [1$\bar{1}$1] direction, in agreement with our experimental observations.

Similarly to the adatom, we expect the spectra pertaining to the spin excitation to result from a complex combination of excitation

Table 1. Ground-state properties of the considered Cr-based nanostructures deposited on the Nb(110) surface. Shown are the magnetic moments per atom M, which are averaged in case of the trimers, the next-nearest neighbor (NNN) isotropic exchange interaction J_1, the next NNN isotropic exchange interaction J_2 along a given direction, and the magnetic anisotropy energy K, per atom. Positive (negative) J corresponds to an antiferromagnetic (FM) coupling, while a positive magnetic anisotropy energy indicates a preference for an in-plane orientation of the spin moments.

	Cr_1	$Cr_2[1\bar{1}0]$	$Cr_2[001]$	$Cr_2[1\bar{1}1]$	$Cr_3[1\bar{1}0]$	$Cr_3[001]$	$Cr_3[1\bar{1}1]$
M [μ_B]	3.53	3.52	3.51	3.53	3.52	3.51	3.54
J_1 [meV]	–	1.24	7.94	−8.95	1.31	7.97	−7.35
J_2 [meV]	–	–	–	–	−0.20	−0.31	−2.38
$\mathcal{K}$ [meV]	0.20	0.20	0.20	0.20	0.2	0.17	0.20

features hosted by majority and minority spin electrons at either side of the bias voltage. This might explain the peculiar spectrum detected experimentally on the [001] dimer (see Fig. 2B), which hosts a deep-like feature offset from zero bias that is induced by the coupling of the two adatoms (see note S10). A similar kink is detected on the theoretical data of the adatom after application of a magnetic field (Fig. 1, E and F).

From trimers to long chains

As identified for the dimers, the distinct spin-excitation spectra of the AFM and FM dimer are triggered by the alignment of their spin moments. To confirm this aspect, we artificially create a trimer along all distinct directions. This breaks the perfect antiferromagnetic balance while it should not strongly affect the excitation behavior of the FM configurations. Scanning tunneling microscope (STM) images for all configurations are shown in Fig. 3A. Because of the C_2 symmetry, the two end atoms (A and A′) can be distinguished from the central one (B) for all trimers. The inelastic STS spectra obtained at 1 T and 600 mK for each Cr atom are shown in Fig. 3B. Similar to the dimers, a clear correlation between the strength of the magnetic coupling (see Table 1) and the deviation of the inelastic STS signal from the single adatom case is visible. Moreover, we also recover similar trends: The $[1\bar{1}0]$ trimer exhibits the weakest magnetic coupling and therefore only a weak deviation from the single adatom spectra is observed, while the observed broadening increases for the stronger coupled trimers along the $[1\bar{1}1]$ and [001] directions. Noteworthy, we find two distinct trends depending on the nature of the magnetic coupling: The ferromagnetic trimer along the $[1\bar{1}1]$ direction shows only a very weak difference between the end atoms (A) and the central atom (B) in contrast to the antiferromagnetic trimers, with the [001] case hosting the largest discrepancy, while the antiferromagnetic trimers show an increased broadening for the central atoms, which is strongest for the [001] case.

To explain the observed spectra theoretically, we exploit the density of spin excitations of the trimers shown in Fig. 3C. For all trimers, the end atoms host a peak close to the excitation energy of the isolated adatom. The ferromagnetic $[1\bar{1}0]$ trimer shows peaks at higher energies depending on the nature of the considered atom. Because of the increased coordination number of the central atom B, its high-energy peak is higher in energy than the one of atom A. For the antiferromagnetically coupled trimers along the [001] and $[1\bar{1}0]$ directions, two fundamentally different spectra are observed depending on whether atom A or B is excited. The low-energy excitations contrast those observed for the dimers, which showed only a single broad feature. The fundamental difference between the antiferromagnetic dimers and trimers is that the net magnetic moment cancels out in the former, while it is finite for the latter. This triggers a mixture of modes similar to those of the ferromagnetic and antiferromagnetic dimers. Thus, unlike the dimers, the trimers can respond to an external magnetic field while preserving their collinear antiferromagnetic configuration. The lowest mode corresponds to a collinear in-phase motion of all three atoms at an energy $\omega \approx 3\gamma\mathcal{K}/M$ (see note S8), and the density of spin excitations in Fig. 3C shows that this mode is possible to be excited via the end atoms A and A′. In contrast, the central atom B only excites the modes at higher energy and with larger broadening, i.e., translating to a larger coupling to electron-hole excitations, which explains the observed inelastic STS signatures in Fig. 3B. By progressively increasing the size of the wires, we recover a spectroscopic behavior similar to that of the trimers (see note S12). We note that a similar sequence of modes was observed in (*17*), which can equivalently be explained in terms of the nodal structure of the collective spin excitations hosted by the nanomagnet.

Spin-resolved spectroscopy

Last, we experimentally scrutinize the spin-resolved spectroscopic signatures for chains oriented along the [001] direction, i.e., when neighboring adatoms are strongly antiferromagnetically coupled (see also related notes S11 and S12). This is a particularly interesting scenario, since the splitting of the zero-bias anomaly is the strongest (see section on dimers). This is expected to result in well-separated spectroscopic signatures for opposite spin channels, a direct result of the magnetic interaction between the adatoms, which renormalizes the spectrum while simultaneously removing the spin degeneracy (*60*). This situation is analog to the theoretical plots presented in Fig. 1F for a single adatom. The coupling between adatoms can be considered as an effective magnetic field. Figure 4A shows the spin-resolved spectroscopic data acquired with a Cr-terminated W tip under a magnetic field strength of 5 T applied perpendicular to the sample surface. Spectra obtained by positioning the tip on top of each one of the adatom in the chain are indicated by numbers. An alternating contrast is clearly visible along the chain, with a slightly different signature for adatoms localized at the end of the chain (numbers 1 and 7 in Fig. 4A), a direct consequence of their different local environment compared to adatoms in the bulk of the chain. The spectral shape is better highlighted in Fig. 4B, which directly compares the spectra acquired on antiferromagnetically coupled adatoms, i.e., numbers 3 and 4 in Fig. 4A. The spectra for opposite

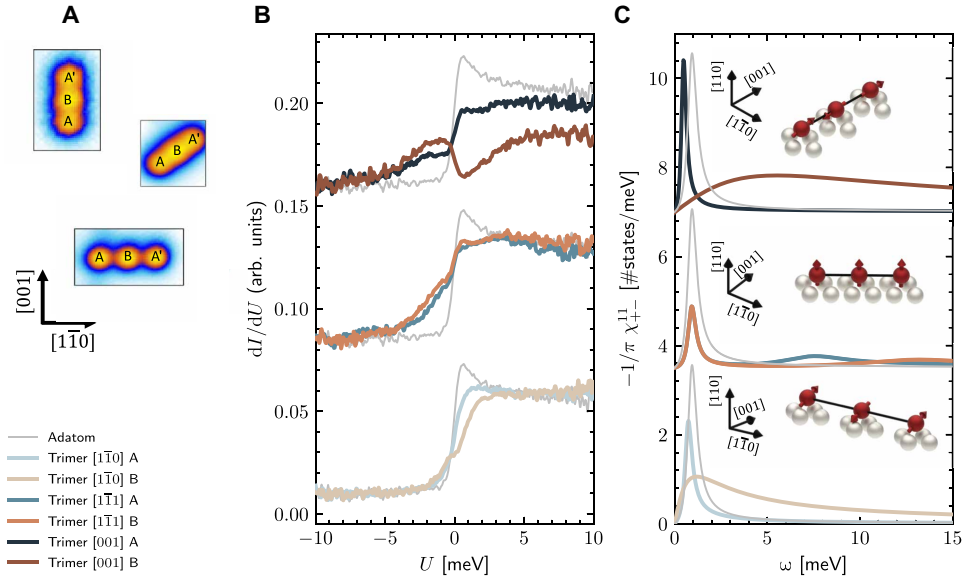

Fig. 3. Cr trimers along the [001], [1$\bar{1}$0], and [1$\bar{1}$1] directions on the Nb(110) surface. (**A**) Illustration of the trimers (STM topography). (**B**) Experimental inelastic STS spectra of the trimers at 1 T (colored lines). The measurements on the single Cr adatom are shown as reference (thin gray lines, see also Fig. 1). (**C**) Magnetic susceptibility obtained from TD-DFT at 5 T. The spectra of atom B in the [1$\bar{1}$0] direction and in the [001] direction are scaled by a factor 10 and 30, respectively. All trimer spectra are vertically shifted to improve visibility. The insets show the magnetic structures obtained from self-consistent noncollinear DFT calculations.

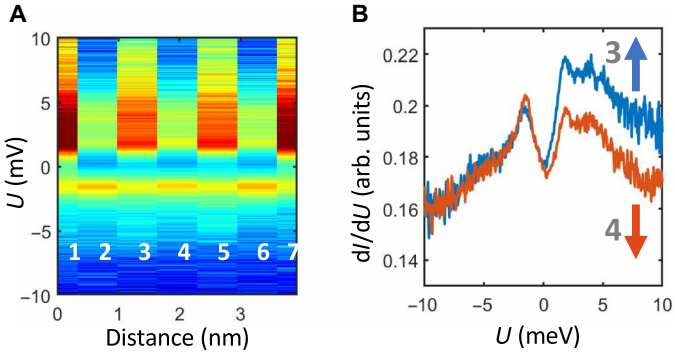

Fig. 4. Spin-polarized STS acquired on a seven-adatom chain along [001]. (**A**) Spectroscopic data collected by positioning the tip on top of each adatom along the chain (see numbers). The data reveal the existence of antiferromagnetic coupling. (**B**) Comparison between the STS spectra acquired on neighboring adatom [3 and 4 in (A)], highlighting the opposite spin contrast. Measurements have been acquired at 5 T with a Cr-terminated tip. Stabilization parameters: $V = -10$ meV, $I = 3$ nA, and modulation $V_{rms} = 200$ μV.

spin channels are in good agreement with the theoretically calculated ones shown in Fig. 1F, i.e., a relatively sharp peak center below the Fermi level, and a broader step-like signature at positive energy.

DISCUSSION

In conclusion, we systematically unveiled zero-bias anomalies in Cr atom nanostructures deposited on the metallic Nb(110) surface. Our inelastic STS measurements reveal an asymmetric single step-like zero-bias feature, which is preserved but can be modulated depending on the strength of the external magnetic field, the size of the nanostructure, and its spatial orientation on the substrate. The latter is used to engineer interatom magnetic coupling to be ferromagnetic or antiferromagnetic. We demonstrated the possibility of tracking these complex spectral line shapes through ab initio simulations combining time-dependent density functional and many-body perturbation theories, evidencing that by constructing the nano-object with the desired magnetic state, one can control the underlying excitation energies and related lifetimes by affecting the number of emitted electron-hole excitations. The emitted spin currents accompanying the electron-hole excitations characterizing each excitation mode might prove useful for spin-pumping nanoscale devices to explore innovative spintronics concepts based on spin-transfer/spin-orbit torques and spin-Hall effects, for the manipulation of quantum spins. Our results shed new light on the interpretation of zero-bias anomalies and pave a way to engineering low-energy features by manipulating the spin excitation spectra by using the underlying magnetic structure.

METHODS

Sample and tip preparation

To obtain an atomically flat and clean substrate, a commercial Nb single crystal polished on one side with (110) surface normal was heated up to 2300 K multiple times by short flashes of electron bombardment and under ultra-high vacuum (UHV) conditions (*46*). The procedure is repeated until the main contaminant oxygen gives way to large areas of clean Nb. In situ deposition of Cr atoms is done by keeping the substrate cold below 15 K to prevent migration and to avoid clustering of adsorbed single atoms. A commercial STM head from Scienta Omicron is used to carry out topographic imaging, STS measurements, and atomic manipulation of Cr adatoms. Data are acquired in 10^{-10} mbar pressure at a temperature of 600 mK

and with an applied external magnetic field of >1 T using an etched tungsten tip characterized on Ag(111). Bringing the tip close to the adatoms by increasing the constant tunneling current set point to about 70 nA at a bias voltage of −5 mV enabled us to drag the Cr single atoms to the desired lattice positions and to isolate all the nanostructures under investigation from surrounding Cr atoms by at least 4 nm.

First-principles calculations

The methodology followed in our work is based on a first-principles approach as implemented in the framework of the scalar-relativistic full-electron Korringa-Kohn-Rostoker Green function augmented self-consistently with spin-orbit interaction (*61*, *62*). The spin excitations are described in a formalism based on TD-DFT (*6*, *57*, *63*, *64*), including spin-orbit interaction. Many-body effects triggered by the presence of spin excitations are approached via the many-body perturbation theory (*49*, *50*, *65*), extended to account for relativistic effects (*40*). The used multiple-scattering theory enables an embedding scheme, which is versatile for the treatment of nanostructures in real space. The local spin density approximation (LSDA) is used for the evaluation of the exchange-correlation potential (*66*), while the full charge density is computed within the atomic-sphere approximation. We assume an angular momentum cutoff at $\ell_{\max} = 3$ for the orbital expansion of the Green function, and when extracting the local density of states, a k-mesh of 450 × 450 is considered. The Cr atoms sit on the hollow stacking site relaxed toward the surface by 20% of the interlayer distance of the underlying Nb(110) surface, as found in previous studies (*47*).

The single-particle Green functions corresponding to the ground state are used for the construction of the tensor of dynamical magnetic susceptibilities, $\underline{\chi}(\omega)$, within TD-DFT (*6*, *57*, *64*), including spin-orbit interaction. In practice, we solve the Dyson-like equation relating the full susceptibility to the Kohn-Sham susceptibility, $\underline{\chi}_{\mathrm{KS}(\omega)}$ as

$$\underline{\chi}(\omega) = \underline{\chi}_{\mathrm{KS}}(\omega) + \underline{\chi}_{\mathrm{KS}}(\omega)\, \underline{\mathcal{K}}\, \underline{\chi}(\omega) \qquad (1)$$

where $\underline{\chi}_{\mathrm{KS}}(\omega)$ describes uncorrelated electron-hole excitations, while $\underline{\mathcal{K}}$ represents the exchange-correlation kernel, taken in adiabatic LSDA [such that this quantity is local in space and frequency independent (*67*)]. The energy gap in the spin excitation spectrum is accurately evaluated using a magnetization sum rule (*6*, *57*, *64*).

The magnetic exchange interactions in the dimers and trimers were obtained using the magnetic force theorem in the frozen-potential approximation and the infinitesimal rotation method (*68*). The on-site magnetic anisotropy of the Cr atoms in all systems is obtained from the method of constraining fields (*69*). More details are given in notes S6 and S7.

Considering the reasonable theoretical recovery of the experimentally observed low-energy anomaly, we discuss here the impact of the assumptions made within the simulations. It is clear that the assumed LSDA is performing well in describing the magnitude of the magnetic anisotropy energy, which dictates the position of the spin excitation, and of the magnetic exchange interactions since the spin-polarized STS experiments are in nice agreement with the ab initio simulations. However, it is very possible that a slight shift in the magnetic anisotropy energy and of the electronic states at the Fermi energy, which defines the lifetime/broadening of the zero-bias anomalies, by changing the exchange and correlation potential could improve the agreement between theory and experiment.

SUPPLEMENTARY MATERIALS

Supplementary material for this article is available at https://science.org/doi/10.1126/sciadv.abi7291

REFERENCES AND NOTES

1. R. Sessoli, D. Gatteschi, A. Caneschi, M. A. Novak, Magnetic bistability in a metal-ion cluster. *Nature* **365**, 141–143 (1993).
2. S. Loth, S. Baumann, C. P. Lutz, D. M. Eigler, A. J. Heinrich, Bistability in atomic-scale antiferromagnets. *Science* **335**, 196–199 (2012).
3. A. A. Khajetoorians, B. Baxevanis, C. Hübner, T. Schlenk, S. Krause, T. O. Wehling, S. Lounis, A. Lichtenstein, D. Pfannkuche, J. Wiebe, R. Wiesendanger, Current-driven spin dynamics of artificially constructed quantum magnets. *Science* **339**, 55–59 (2013).
4. I. G. Rau, S. Baumann, S. Rusponi, F. Donati, S. Stepanow, L. Gragnaniello, J. Dreiser, C. Piamonteze, F. Nolting, S. Gangopadhyay, O. R. Albertini, R. M. Macfarlane, C. P. Lutz, B. A. Jones, P. Gambardella, A. J. Heinrich, H. Brune, Reaching the magnetic anisotropy limit of a 3D metal atom. *Science* **344**, 988–992 (2014).
5. B. W. Heinrich, L. Braun, J. I. Pascual, K. J. Franke, Protection of excited spin states by a superconducting energy gap. *Nat. Phys.* **9**, 765–768 (2013).
6. S. Lounis, A. T. Costa, R. B. Muniz, D. L. Mills, Dynamical magnetic excitations of nanostructures from first principles. *Phys. Rev. Lett.* **105**, 187205 (2010).
7. A. A. Khajetoorians, S. Lounis, B. Chilian, A. T. Costa, L. Zhou, D. L. Mills, J. Wiebe, R. Wiesendanger, Itinerant nature of atom-magnetization excitation by tunneling electrons. *Phys. Rev. Lett.* **106**, 037205 (2011).
8. W. Paul, K. Yang, S. Baumann, N. Romming, T. Choi, C. P. Lutz, A. J. Heinrich, Control of the millisecond spin lifetime of an electrically probed atom. *Nat. Phys.* **13**, 403–407 (2017).
9. M. Ternes, Spin excitations and correlations in scanning tunneling spectroscopy. *New J. Phys.* **17**, 063016 (2015).
10. F. Donati, S. Rusponi, S. Stepanow, C. Wäckerlin, A. Singha, L. Persichetti, R. Baltic, K. Diller, F. Patthey, E. Fernandes, J. Dreiser, Z. Sljivan˘canin, K. Kummer, C. Nistor, P. Gambardella, H. Brune, Magnetic remanence in single atoms. *Science* **352**, 318–321 (2016).
11. S. Baumann, W. Paul, T. Choi, C. P. Lutz, A. Ardavan, A. J. Heinrich, Electron paramagnetic resonance of individual atoms on a surface. *Science* **350**, 417–420 (2015).
12. D.-J. Choi, N. Lorente, J. Wiebe, K. von Bergmann, A. F. Otte, A. J. Heinrich, Colloquium: Atomic spin chains on surfaces. *Rev. Mod. Phys.* **91**, 041001 (2019).
13. G. Serrano, L. Poggini, M. Briganti, A. L. Sorrentino, G. Cucinotta, L. Malavolti, B. Cortigiani, E. Otero, P. Sainctavit, S. Loth, F. Parenti, A.-L. Barra, A. Vindigni, A. Cornia, F. Totti, M. Mannini, R. Sessoli, Quantum dynamics of a single molecule magnet on superconducting pb(111). *Nat. Mater.* **19**, 546–551 (2020).
14. V. Madhavan, W. Chen, T. Jamneala, M. F. Crommie, N. S. Wingreen, Tunneling into a single magnetic atom: Spectroscopic evidence of the Kondo resonance. *Science* **280**, 567–569 (1998).
15. C. F. Hirjibehedin, C. P. Lutz, A. J. Heinrich, Spin coupling in engineered atomic structures. *Science* **312**, 1021–1024 (2006).
16. S. Nadj-Perge, I. K. Drozdov, J. Li, H. Chen, S. Jeon, J. Seo, A. H. MacDonald, B. A. Bernevig, A. Yazdani, Observation of majorana fermions in ferromagnetic atomic chains on a superconductor. *Science* **346**, 602–607 (2014).
17. A. Spinelli, B. Bryant, F. Delgado, J. Fernandez-Rossier, A. F. Otte, Imaging of spin waves in atomically designed nanomagnets. *Nat. Mater.* **13**, 782–785 (2014).
18. R. Toskovic, R. van den Berg, A. Spinelli, I. S. Eliens, B. van den Toorn, B. Bryant, J. S. Caux, A. F. Otte, Atomic spin-chain realization of a model for quantum criticality. *Nat. Phys.* **12**, 656–660 (2016).
19. W. Wernsdorfer, R. Sessoli, Quantum phase interference and parity effects in magnetic molecular clusters. *Science* **284**, 133–135 (1999).
20. J. Lehmann, A. Gaita-Ariño, E. Coronado, D. Loss, Spin qubits with electrically gated polyoxometalate molecules. *Nat. Nanotechnol.* **2**, 312–317 (2007).
21. A. A. Khajetoorians, J. Wiebe, B. Chilian, R. Wiesendanger, Realizing all-spin–based logic operations atom by atom. *Science* **332**, 1062–1064 (2011).
22. J. Hermenau, J. Ibañez-Azpiroz, C. Hübner, A. Sonntag, B. Baxevanis, K. T. Ton, M. Steinbrecher, A. A. Khajetoorians, M. dos Santos Dias, S. Blügel, R. Wiesendanger, S. Lounis, J. Wiebe, A gateway towards non-collinear spin processing using three-atom magnets with strong substrate coupling. *Nat. Commun.* **8**, 642 (2017).
23. P. Willke, W. Paul, F. D. Natterer, K. Yang, Y. Bae, T. Choi, J. Fernandez-Rossier, A. J. Heinrich, C. P. Lutz, Probing quantum coherence in single-atom electron spin resonance. *Science* **4**, eaaq1543 (2018).
24. A. J. Heinrich, J. A. Gupta, C. P. Lutz, D. M. Eigler, Single-Atom Spin-Flip Spectroscopy. **306**, 466–469 (2004).

25. J. Fernandez-Rossier, Theory of single-spin inelastic tunneling spectroscopy. *Phys. Rev. Lett.* **102**, 256802 (2009).
26. B. Chilian, A. A. Khajetoorians, S. Lounis, A. T. Costa, D. L. Mills, J. Wiebe, R. Wiesendanger, Anomalously large *g* factor of single atoms adsorbed on a metal substrate. *Phys. Rev. B* **84**, 212401 (2011).
27. A. A. Khajetoorians, T. Schlenk, B. Schweflinghaus, M. dos Santos Dias, M. Steinbrecher, M. Bouhassoune, S. Lounis, J. Wiebe, R. Wiesendanger, Spin excitations of individual Fe atoms on Pt(111): Impact of the site-dependent giant substrate polarization. *Phys. Rev. Lett.* **111**, 157204 (2013).
28. B. Bryant, A. Spinelli, J. J. T. Wagenaar, M. Gerrits, A. F. Otte, Local control of single atom magnetocrystalline anisotropy. *Phys. Rev. Lett.* **111**, 127203 (2013).
29. J. C. Oberg, M. R. Calvo, F. Delgado, M. Moro-Lagares, D. Serrate, D. Jacob, J. Fernández-Rossier, C. F. Hirjibehedin, Control of single-spin magnetic anisotropy by exchange coupling. *Nat. Nanotechnol.* **9**, 64–68 (2014).
30. B. C. Stipe, M. A. Rezaei, W. Ho, Single-molecule vibrational spectroscopy and microscopy. *Science* **280**, 1732–1735 (1998).
31. M. Pohlit, S. Rößler, Y. Ohno, H. Ohno, S. von Molnar, Z. Fisk, J. Müller, S. Wirth, Evidence for ferromagnetic clusters in the colossal-magnetoresistance material EuB6. *Phys. Rev. Lett.* **120**, 257201 (2018).
32. D. Pommier, R. Bretel, L. E. P. López, F. Fabre, A. Mayne, E. Boer-Duchemin, G. Dujardin, G. Schull, S. Berciaud, E. Le Moal, Scanning tunneling microscope-induced excitonic luminescence of a two-dimensional semiconductor. *Phys. Rev. Lett.* **123**, 027402 (2019).
33. J. Kondo, Resistance minimum in dilute magnetic alloys. *Prog. Theor. Exp. Phys.* **32**, 37–49 (1964).
34. A. C. Hewson, *The Kondo Problem to Heavy Fermions, Cambridge Studies in Magnetism* (Cambridge Univ. Press, 1993).
35. N. Knorr, M. A. Schneider, L. Diekhöner, P. Wahl, K. Kern, Kondo effect of single Co adatoms on Cu surfaces. *Phys. Rev. Lett.* **88**, 096804 (2002).
36. M. Ternes, A. J. Heinrich, W.-D. Schneider, Spectroscopic manifestations of the Kondo effect on single adatoms. *J. Phys. Condens. Matter* **21**, 053001 (2008).
37. A. F. Otte, M. Ternes, K. von Bergmann, S. Loth, H. Brune, C. P. Lutz, C. F. Hirjibehedin, A. J. Heinrich, The role of magnetic anisotropy in the Kondo effect. *Nat. Phys.* **4**, 847–850 (2008).
38. T.-M. Chen, A. C. Graham, M. Pepper, I. Farrer, D. A. Ritchie, Non-Kondo zero-bias anomaly in quantum wires. *Phys. Rev. B* **79**, 153303 (2009).
39. S. Sarkozy, F. Sfigakis, K. Das Gupta, I. Farrer, D. A. Ritchie, G. A. C. Jones, M. Pepper, Zero-bias anomaly in quantum wires. *Phys. Rev. B* **79**, 161307 (2009).
40. J. Bouaziz, J. Ibañez Azpiroz, F. S. M. Guimarães, S. Lounis, Zero-point magnetic exchange interactions. *Phys. Rev. Res.* **2**, 043357 (2020).
41. B. Surer, M. Troyer, P. Werner, T. O. Wehling, A. M. Läuchli, A. Wilhelm, A. I. Lichtenstein, Multiorbital Kondo physics of Co in Cu hosts. *Phys. Rev. B* **85**, 085114 (2012).
42. H. T. Dang, M. dos Santos Dias, A. Liebsch, S. Lounis, Strong correlation effects in theoretical STM studies of magnetic adatoms. *Phys. Rev. B* **93**, 115123 (2016).
43. K. Nagaoka, T. Jamneala, M. Grobis, M. F. Crommie, Temperature dependence of a single Kondo impurity. *Phys. Rev. Lett.* **88**, 077205 (2002).
44. K. J. Franke, G. Schulze, J. I. Pascual, Competition of superconducting phenomena and Kondo screening at the nanoscale. *Science* **332**, 940–944 (2011).
45. J. Kügel, M. Karolak, J. Senkpiel, P.-J. Hsu, G. Sangiovanni, M. Bode, Relevance of hybridization and filling of 3D orbitals for the Kondo effect in transition metal phthalocyanines. *Nano Lett.* **14**, 3895–3902 (2014).
46. A. B. Odobesko, S. Haldar, S. Wilfert, J. Hagen, J. Jung, N. Schmidt, P. Sessi, M. Vogt, S. Heinze, M. Bode, Preparation and electronic properties of clean superconducting nb(110) surfaces. *Phys. Rev. B* **99**, 115437 (2019).
47. F. Küster, A. M. Montero, F. S. M. Guimarães, S. Brinker, S. Lounis, S. S. P. Parkin, P. Sessi, Correlating Josephson supercurrents and Shiba states in quantum spins unconventionally coupled to superconductors. *Nat. Commun.* **12**, 1108 (2021).
48. F. Küster, S. Brinker, S. Lounis, S. S. P. Parkin, P. Sessi, Long range and highly tunable interaction between local spins coupled to a superconducting condensate. *Nat. Commun.* **12**, 6722 (2021).
49. B. Schweflinghaus, M. dos Santos Dias, A. T. Costa, S. Lounis, Renormalization of electron self-energies via their interaction with spin excitations: A first-principles investigation. *Phys. Rev. B* **89**, 235439 (2014).
50. B. Schweflinghaus, M. dos Santos Dias, S. Lounis, Observing spin excitations in *3D* transition-metal adatoms on Pt(111) with inelastic scanning tunneling spectroscopy: A first-principles perspective. *Phys. Rev. B* **93**, 035451 (2016).
51. D. L. Mills, P. Lederer, Dynamical properties of magnetic impurities in transition metals. *Phys. Rev.* **160**, 590–599 (1967).
52. Y. Tserkovnyak, A. Brataas, G. E. W. Bauer, Spin pumping and magnetization dynamics in metallic multilayers. *Phys. Rev. B* **66**, 224403 (2002).
53. W. Zhang, W. Han, X. Jiang, S.-H. Yang, S. S. P. Parkin, Role of transparency of platinum–ferromagnet interfaces in determining the intrinsic magnitude of the spin Hall effect. *Nat. Phys.* **11**, 496–502 (2015).
54. J.-C. Rojas-Sánchez, N. Reyren, P. Laczkowski, W. Savero, J.-P. Attané, C. Deranlot, M. Jamet, J.-M. George, L. Vila, H. Jaffrès, Spin pumping and inverse spin Hall effect in platinum: The essential role of spin-memory loss at metallic interfaces. *Phys. Rev. Lett.* **112**, 106602 (2014).
55. L. D. Landau, E. Lifshitz, On the theory of the dispersion of magnetic permeability in ferromagnetic bodies. *Phys. Z. Sowjet.* **8**, 153 (1935).
56. T. L. Gilbert, A phenomenological theory of damping in ferromagnetic materials. *IEEE Trans. Magn.* **40**, 3443–3449 (2004).
57. M. dos Santos Dias, B. Schweflinghaus, S. Blügel, S. Lounis, Relativistic dynamical spin excitations of magnetic adatoms. *Phys. Rev. B* **91**, 075405 (2015).
58. P. Wahl, L. Diekhöner, M. A. Schneider, L. Vitali, G. Wittich, K. Kern, Kondo temperature of magnetic impurities at surfaces. *Phys. Rev. Lett.* **93**, 176603 (2004).
59. L. Schneider, P. Beck, J. Wiebe, R. Wiesendanger, Atomic-scale spin-polarization maps using functionalized superconducting probes. *Sci. Adv.* **7**, abd7302 (2021).
60. Y.-S. Fu, Q.-K. Xue, R. Wiesendanger, Spin-resolved splitting of Kondo resonances in the presence of RKKY-type coupling. *Phys. Rev. Lett.* **108**, 087203 (2012).
61. N. Papanikolaou, R. Zeller, P. H. Dederichs, Conceptual improvements of the KKR method. *J. Phys. Condens. Matter* **14**, 2799–2823 (2002).
62. D. S. G. Bauer, Development of a relativistic full-potential first-principles multiple scattering Green function method applied to complex magnetic textures of nanostructures at surfaces. Forschungszentrum Jülich (2014).
63. S. Lounis, A. T. Costa, R. B. Muniz, D. L. Mills, Theory of local dynamical magnetic susceptibilities from the Korringa-Kohn-Rostoker Green function method. *Phys. Rev. B* **83**, 035109 (2011).
64. S. Lounis, M. dos Santos Dias, B. Schweflinghaus, Transverse dynamical magnetic susceptibilities from regular static density functional theory: Evaluation of damping and g shifts of spin excitations. *Phys. Rev. B* **91**, 104420 (2015).
65. J. Ibañez Azpiroz, M. dos Santos Dias, B. Schweflinghaus, S. Blügel, S. Lounis, Tuning paramagnetic spin excitations of single adatoms. *Phys. Rev. Lett.* **119**, 017203 (2017).
66. S. H. Vosko, L. Wilk, M. Nusair, Accurate spin-dependent electron liquid correlation energies for local spin density calculations: A critical analysis. *Can. J. Phys.* **58**, 1200–1211 (1980).
67. E. K. U. Gross, W. Kohn, Local density-functional theory of frequency-dependent linear response. *Phys. Rev. Lett.* **55**, 2850–2852 (1985).
68. H. Ebert, S. Mankovsky, Anisotropic exchange coupling in diluted magnetic semiconductors: Ab initio spin-density functional theory. *Phys. Rev. B* **79**, 045209 (2009).
69. S. Brinker, M. dos Santos Dias, S. Lounis, The chiral biquadratic pair interaction. *N. J. Phys.* **21**, 083015 (2019).

Acknowledgments: S.B. and S.L. thank M. dos Santos Dias, A. M. Montero, and Filipe S. M. Guimarães for discussions. **Funding:** This work is supported by the European Research Council (ERC) under the European Union's Horizon 2020 Research and Innovation Programme (ERC-consolidator grant 681405, DYNASORE). We acknowledge the computing time granted by the JARA-HPC Vergabegremium and VSR commission on the supercomputer JURECA at Forschungszentrum Jülich. **Author contributions:** P.S. and S.L. initiated, designed, and supervised the project. F.K. performed all the STM measurements supervised by S.S.P.P. and P.S. S.B. performed the ab initio simulations supervised by S.L. S.B. and S.L. wrote the manuscript to which all authors contributed via discussions and corrections. **Competing interests:** The authors declare that they have no competing interests. **Data and materials availability:** All data needed to evaluate the conclusions in the paper are present in the paper and/or the Supplementary Materials.

Submitted 26 March 2021
Accepted 6 December 2021
Published 26 January 2022
10.1126/sciadv.abi7291